Atmos. Chem. Phys. Discuss., 15, 19835–19872, 2015
www.atmos-chem-phys-discuss.net/15/19835/2015/
doi:10.5194/acpd-15-19835-2015

Atmospheric Chemistry and Physics Discussions

Variation of the radiative properties during black carbon aging: theoretical and experimental intercomparison

C. He[1,2], K.-N. Liou[1,2], Y. Takano[1,2], R. Zhang[3], M. L. Zamora[3], P. Yang[3], Q. Li[1,2], and L. R. Leung[4]

[1]Department of Atmospheric and Oceanic Sciences, University of California, Los Angeles (UCLA), 90095, USA
[2]Joint Institute for Regional Earth System Science and Engineering, University of California, Los Angeles (UCLA), 90095, USA
[3]Department of Atmospheric Sciences, Texas A&M, College Station, 77845, USA
[4]Pacific Northwest National Laboratory, Richland, WA 99352, USA

Received: 8 June 2015 – Accepted: 30 June 2015 – Published: 20 July 2015

Correspondence to: C. He (cenlinhe@atmos.ucla.edu)

Published by Copernicus Publications on behalf of the European Geosciences Union.

Abstract

A theoretical black carbon (BC) aging model is developed to account for three typical evolution stages, namely, freshly emitted aggregates, coated BC by soluble material, and BC particles undergoing further hygroscopic growth. The geometric-optics surface-wave (GOS) approach is employed to compute the BC single-scattering properties at each aging stage, which are subsequently compared with laboratory measurements. Theoretical calculations are consistent with measurements in extinction and absorption cross sections for fresh BC aggregates, but overestimate the scattering cross sections for BC mobility diameters of 155, 245, and 320 nm, because of uncertainties associated with theoretical calculations for small particles as well as laboratory scattering measurements. The measured optical cross sections for coated BC by sulfuric acid and for those undergoing further hygroscopic growth are captured by theoretical calculations using a concentric core-shell structure, with differences of less than 20 %. This suggests that the core-shell shape represents the realistic BC coating morphology reasonably well in this case, which is consistent with the observed strong structure compaction during aging. We find that the absorption and scattering properties of fresh BC aggregates vary by up to 60 % due to uncertainty in the BC refractive index, which, however, is a factor of two smaller in the case of coated BC particles. Sensitivity analyses on the BC morphology show that the optical properties of fresh BC aggregates are more sensitive to fractal dimension than primary spherule size. The absorption and scattering cross sections of coated BC particles vary by more than a factor of two due to different coating structures. We find an increase of 20–250 % in absorption and a factor of 3–15 in scattering during aging, significantly depending on coating morphology and aging stages. Applying the aging model to CalNex 2010 field measurements, we show that the resulting BC direct radiative forcing (DRF) first increases from 1.5 to 1.7 $W m^{-2}$ and subsequently decreases to 1.0 $W m^{-2}$ during the transport from the Los Angeles Basin to downwind regions, as a result of the competition between absorption enhancement due to coating and dilution of BC concentration. The BC DRF can vary

ACPD
15, 19835–19872, 2015

by up to a factor of two due to differences in BC coating morphology. Thus, an accurate estimate of BC DRF requires the incorporation of a dynamic BC aging process that accounts for realistic morphology in climate models, particularly for the regional analysis with high atmospheric heterogeneity.

1 Introduction

Black carbon (BC) has been identified as the second most important anthropogenic global warming agent in the atmosphere by virtue of its strong absorption of solar radiation and its role as cloud condensation nuclei (CCN) in cloud formation (Ramanathan and Carmichael, 2008; Bond et al., 2013; Wang et al., 2013; Jacobson, 2014). The BC climatic effects are significantly influenced by BC aging process in the atmosphere, which transforms BC from an external to internal mixing state (Schwarz et al., 2008; China et al., 2013) and increases its hygroscopicity (Zhang et al., 2008; Popovicheva et al., 2011) and light absorption (Jacobson, 2001; Scarnato et al., 2013).

Freshly emitted BC particles are mostly hydrophobic and externally mixed with other aerosol constituents (Zuberi et al., 2005; Zhang et al., 2008). BC agglomerates shortly after emission to form irregular aggregates because of multi-phase processes (Zhang et al., 2008; Pagels et al., 2009; Xue et al., 2009). Early studies have found that BC particles age in the atmosphere through condensation and coagulation processes (e.g., Heintzenberg and Covert, 1984; Heintzenberg, 1989). Recent studies confirmed that BC becomes coated by water-soluble material during atmospheric aging, including condensation of sulfate, nitrate, and organics (Schnaiter et al., 2003; Moteki et al., 2007), coagulation with preexisting aerosols (Johnson et al., 2005; Kondo et al., 2011), and heterogeneous reactions with gaseous oxidants (Zuberi et al., 2005; Khalizov et al., 2010; Zhang et al., 2012). At the same time, BC aggregates also exhibit considerable restructuring and compaction (Weingartner et al., 1997; Saathoff et al., 2003; Zhang et al., 2008), which significantly alters BC morphology (Adachi and Buseck, 2013; China et al., 2015). Aged BC particles experience hygroscopic growth and acti-

ACPD
15, 19835–19872, 2015

vate efficiently as CCN (Zuberi et al., 2005; Zhang et al., 2008). The hygroscopic growth of BC particles depends on its initial size, condensed soluble material mass, surface chemical property, and ambient relative humidity (RH) (Zhang et al., 2008; Khalizov et al., 2009b; Popovicheva et al., 2011).

A number of laboratory experiments have been conducted to investigate the effects of atmospheric aging on BC radiative properties. Gangl et al. (2008) showed that internal BC-wax mixture amplifies BC absorption coefficient by a factor of 1.8. Such significant increase in BC absorption has also been observed for BC coated by sulfuric acid (Zhang et al., 2008) and some organics (Shiraiwa et al., 2010), while Saathoff et al. (2003) found that organic coating of BC particles only increases absorption by 30 %. Xue et al. (2009) and Qiu et al. (2012) showed a less than 20 % increase in BC absorption for organic coating, which depends on organic species and coating thickness. The disagreement among different laboratory experiments demonstrates large uncertainties associated with BC radiative properties during aging.

Field measurements have also revealed substantial variation in BC optical properties during atmospheric aging. Bond and Bergstrom (2006) showed that observed BC mass absorption cross sections (MAC) vary by more than a factor of two (mostly 5–13 $m^2\,g^{-1}$) under different atmospheric conditions. Schwarz et al. (2008) applied a concentric core-shell structure to observed coated BC particles using the Mie calculation (Toon and Ackerman, 1981) and found that BC coating increases column absorption by 30–50 % in the tropical atmosphere. Moffett and Prather (2009) measured internally mixed BC particles in Riverside and Mexico City and showed that the concentric core-shell structure of coated BC results in up to a 60 % increase in absorption compared with freshly emitted BC. Similar increases in absorption have also been directly observed for the internal mixing of biomass-burning BC (Lack et al., 2012). However, Cappa et al. (2012) reported that the observed BC absorption increased only by 6 % due to internal mixing during aircraft measurements over California. This implies that BC coating structures are more complex in reality than the idealized concentric core-shell shape.

ACPD
15, 19835–19872, 2015

Adachi et al. (2010) found that many BC particles embedded within host material are chainlike aggregates locating in off-center positions, based on transmission electron microscope (TEM) observations for samples collected from Mexico City. Using the discrete dipole approximation (DDA) method developed by Draine and Flatau (1994), Adachi et al. showed that a more realistic BC coating morphology results in 20–40 % less absorption at visible wavelengths than a concentric core-shell shape. Sedlacek et al. (2012) found that more than 60 % of coated BC particles have non-core-shell structures in a biomass burning plume. During the California Research at the Nexus of Air Quality and Climate Change (CalNex) 2010 aircraft campaign, Adachi and Buseck (2013) further observed that many BC particles are only attached to host material instead of fully embedded within them, leading to only a slight increase in BC absorption. They concluded that the complex mixing structure of BC particles could explain a smaller absorption amplification by BC coating determined from observations than the results computed from an idealized core-shell model. China et al. (2013, 2015) classified the observed irregular BC coating shapes into four types: embedded (heavily coated), thinly coated, partly coated, and partially encapsulated. These complex coating structures substantially affect BC optical properties (e.g., Videen et al., 1994; Liu and Mishchenko, 2007; Kahnert et al., 2013), which is one of the most important uncertainty sources in evaluating BC direct radiative forcing (DRF) (Bond et al., 2013). Thus, a reliable estimate of BC DRF requires a quantitative understanding of the evolution of BC radiative properties under the influence of various morphology during atmospheric aging.

In this study, we have developed a theoretical BC aging model based on the current understanding of BC aging process, which accounts for three major stages, namely, freshly emitted aggregates, coated BC by soluble material, and BC particles undergoing further hygroscopic growth. We apply the geometric-optics surface-wave (GOS) approach to compute light absorption and scattering of BC particles at each aging stage. The theoretical calculations are compared with laboratory measurements, followed by a systematic evaluation of uncertainties associated with BC morphology and

ACPD
15, 19835–19872, 2015

refractive index. We further apply the aging model to the CalNex 2010 field campaign to evaluate the evolution of BC DRF over southern California by coupling with a radiative transfer model (RTM) for analysis. Finally, we discuss the implication of model results for BC DRF assessment.

2 Methods

2.1 A theoretical BC aging model

Based on the current knowledge of BC atmospheric aging, we have developed a theoretical model accounting for three major BC aging stages, as depicted in Fig. 1. Stage I represents freshly emitted BC aggregates that are externally mixed with other particles. Stage II represents BC particles coated by water-soluble aerosol constituents through condensation, coagulation, and/or heterogeneous oxidations. Stage III represents BC particles coated by both soluble material and water through hygroscopic growth. According to atmospheric observations, six typical BC coating structures have been considered for stages II and III in this study (Fig. 1), including embedded (i.e., concentric core-cell, off-center core-shell, and closed-cell), partially encapsulated, and partly coated (i.e., open-cell and externally attached) structures following the classification presented in China et al. (2013, 2015). The concentric and off-center core-shell structures (Martin et al., 1998; Sedlacek et al., 2012) are a result of considerable collapse of BC aggregates into more compact and spherical clusters when fully engulfed in coating material (Zhang et al., 2008). The closed-cell structure is an example where coating material not only covers the outer layers of BC aggregates but also fills the internal voids among primary spherules (Strawa et al., 1999). The partially encapsulated structure is formed when only a part of BC aggregate merges inside coating material (China et al., 2015). The open-cell and externally attached structures are produced by coating material sticking to a part of BC aggregates' surface (Stratmann et al., 2010;

ACPD
15, 19835–19872, 2015

China et al., 2015). Further hygroscopic growth of BC particles after stage III could lead to the formation of cloud droplets, a subject beyond the scope of the present study.

2.2 Laboratory measurements

The physical and radiative properties of BC particles during aging after exposure to sulfuric acid (H_2SO_4) under various RH conditions (5–80 %) have been measured in the laboratory by Zhang et al. (2008) and Khalizov et al. (2009a). BC aggregates were generated by incomplete combustion of propane in a laminar diffusion burner (Santoro et al., 1983) and sampled by a pinhole diluter (Kasper et al., 1997). A tandem differential mobility analyzer (TDMA) system was used to produce singly-charged mobility-classified BC particles, followed by a coating chamber with controlled RH and H_2SO_4 vapor concentrations at room temperatures (299 ± 1 K). The BC mass and size growth due to H_2SO_4 and water vapor (H_2O) condensation during aging were measured by an aerosol particle mass (APM) analyzer and TDMA, respectively. The effective density and fractal dimension (D_f) of BC particles were derived from the measured BC mobility diameter (D_{BC}) and mass (see Eqs. 1 and 2 in Zhang et al., 2008). The compaction and restructuring of BC aggregates were captured by a TEM (see Fig. 1 in Zhang et al., 2008). BC extinction and scattering cross sections were measured at 532 nm wavelength by a cavity ring-down spectrometer (CRDS) and an integrating nephelometer, respectively. The absorption cross section was determined from the resulting difference between extinction and scattering cross sections. Khalizov et al. (2009a) showed that the experimental uncertainties associated with instrument calibration, relative humidity, and particle size measurements were within 10 %, which excludes the contribution from multiply charged particles, while the scattering measurements of freshly emitted BC aggregates were associated with high uncertainty. More details in laboratory experiments have been presented in Zhang et al. (2008) and Khalizov et al. (2009a). Three experimental cases with initial D_{BC} of 155, 245, and 320 nm were used in this study (see Table 1). In each case, BC particles exposed to H_2SO_4 vapor (1.4×10^{10} molecules cm^{-3})

ACPD
15, 19835–19872, 2015

at 5 and 80 % RH were used to represent coated BC at stages II and III (see Sect. 2.1), respectively.

2.3 Geometric-optics surface-wave (GOS) approach

We employed the GOS approach developed by Liou et al. (2011, 2014), which explicitly treats fractal aggregates and various coating structures, to compute absorption and scattering properties of BC particles at three aging stages. In the GOS approach, a stochastic procedure developed by Liou et al. (2011) is applied to simulate homogeneous aggregates and coated particles with different shapes in a 3-D coordinate system. In this study, we have extended the original stochastic process to generate more complex coating morphology, including the partially encapsulated and externally attached structures (see Figs. S1–S6 in the Supplement). Once the particle shape and composition are determined by the stochastic procedure, the reflection and refraction of particles are computed with the hit-and-miss Monte Carlo photon tracing technique. The extinction and absorption cross sections are derived following a ray-by-ray integration approach (Yang and Liou, 1997). Diffraction by randomly oriented nonspherical particles is computed on the basis of Babinet's principle and photon-number weighted geometric cross sections. The GOS approach accounts for the interaction of incident waves at grazing angles near the particle edge and propagating along the particle surface into shadow regions, referred to as the surface wave, using the formulation developed by Nussenzveig and Wiscombe (1980) for spheres as the basis for physical adjustments and application to nonspherical particles (Liou et al., 2010, 2011). The concept of the GOS approach is graphically displayed in Fig. 2 and it is designed for computations of absorption and extinction cross sections and asymmetry factors in line with experimental results.

Liou et al. (2010, 2011) and Takano et al. (2013) demonstrated that the single-scattering properties of aerosols with different sizes and shapes determined from the GOS approach compare reasonably well with those determined from the Finite Difference Time Domain (FDTD) method (Yang and Liou, 1996) and DDA (Draine and Flatau,

ACPD
15, 19835–19872, 2015

1994) for column and plate ice crystals, the superposition T-matrix method (Mackowski and Mishchenko, 1996) for fractal aggregates, and the Lorenz–Mie model (Toon and Ackerman, 1981) for a concentric core-shell shape. Moreover, compared with other numerical methods, the GOS approach can be applied to a wider range of particle sizes, shapes, and coating morphology with a high computational efficiency, including very large particles (e.g., ∼ 100–1000 µm snowflakes) and complex multiple inclusions of aerosols within irregular snow grains (Liou et al., 2014; He et al., 2014), in which the FDTD, DDA, and T-matrix methods have not been able to apply. As stated previously, the GOS approach has been developed specifically for extinction and absorption cross sections and the asymmetry factor, but not for scattering phase matrix calculations. Also, due to the approximation in the use of geometric photon tracing, the GOS approach has limitation and uncertainty for application to size parameters much smaller than 1. To supplement GOS, we have developed the Rayleigh–Gan–Debye (RGD) approximation coupled with GOS for very small particles, which has been cross-validated with the superposition T-matrix method (Takano et al., 2013). The combined GOS/RGD approach can be applied to size parameters covering 0.1 to 1000.

2.4 Theoretical calculations

We used BC physical properties measured from laboratory experiments (see Sect. 2.2) as input to theoretical calculations (see Table 1). In standard calculations, the freshly emitted BC aggregates (stage I) were assumed to be comprised of primary spherules with a diameter of 15 nm measured from the experiments and were constructed by the GOS stochastic procedure to reproduce the measured mass and fractal dimension (= 2.1) of BC aggregates. The BC mass was the product of measured BC effective densities and mobility volumes. The mass of H_2SO_4 coating on BC at stage II was derived from the observed relationship between condensed H_2SO_4 mass and particle diameter at 5 % RH. The mass of H_2O condensed on H_2SO_4-coated BC at stage III was derived from the measured hygroscopic mass growth ratio of H_2SO_4-coated BC at 80 % RH. In standard calculations, we used a concentric core-shell structure for

ACPD
15, 19835–19872, 2015

coated BC particles at stages II and III because of the strong particle compaction during aging based on laboratory observations (Zhang et al., 2008). Thus, BC core size and coating thickness were computed from the mass of BC and H_2SO_4/H_2O coating. The refractive index (RI) of H_2SO_4–H_2O coating at stage III was derived as the volume-weighted RI of H_2SO_4 and H_2O. We used a BC RI of 1.95–0.79i recommended by Bond and Bergstrom (2006) and a BC density of 1.77 g cm^{-3} suggested by Zhang et al. (2008). Under the preceding conditions, computations of BC optical properties at 532 nm wavelength were carried out for comparison with laboratory measurements.

In addition, we conducted four sensitivity calculations for stage I and six sensitivity calculations for stages II and III to quantify uncertainties associated with BC RI and morphology (see Table 1). In the first sensitivity calculation for each aging stage, a lower bound of BC RI of 1.75–0.63i recommended by Bond and Bergstrom (2006) was used. For other three sensitivity tests on morphology effects at stage I, we increased BC fractal dimension from 2.1 to 2.5 and primary spherules diameter from 15 to 20 nm without changing BC mass, and replaced BC aggregates with a single volume-equivalent sphere, respectively. We then applied five types of BC coating structures, including off-center core-shell, closed-cell, open-cell, partially encapsulated, and externally attached structures (see Fig. 1 and Sect. 2.1), and conducted five additional sensitivity calculations for both stages II and III. Specifically, the off-center core-shell structure assumes a spherical BC core internally tangent to the particle surface with the same size as the concentric core-shell structure used in standard calculations. The closed-cell structure assumes that all primary spherules have the same concentric core-shell shape with a BC core diameter of 15 nm. The open-cell structure also assumes a diameter of 15 nm for all primary spherules, which are either pure BC or pure coating material. Both closed- and open-cell structures were constructed to have the same fractal dimension as measured in the experiments. The partially encapsulated structure assumes that a random part of BC aggregates is inside a spherical coating particle (Figs. S1–S6), while the externally attached structure assumes that

ACPD
15, 19835–19872, 2015

a single spherical coating particle is randomly sticking to a part of BC aggregate's surface (Figs. S1–S6). BC primary spherules in both structures have diameters of 15 nm.

2.5 Application to field measurements

We utilized BC measurements from the CalNex aircraft campaign conducted in May 2010 (http://www.esrl.noaa.gov/csd/calnex/) as input to the aging model with GOS approach to compute the evolution of BC optical properties and DRF during the transport from the Los Angeles (LA) Basin to downwind regions. The BC particle size, coating thickness and fraction, coating composition, and vertical profile have been measured during the CalNex campaign (Metcalf et al., 2012), which were used to drive theoretical calculations. We used an aggregate structure for uncoated BC and a concentric core-shell structure for coated BC. To quantify uncertainties associated with BC RI and morphology, we have conducted calculations with BC RI of 1.95–0.79*i* and 1.75–0.63*i* and different particle structures for uncoated/coated BC as used in the proceeding comparison with laboratory experiments (see Sect. 2.4). Since the CalNex 2010 measurements of BC vertical distribution only covers an altitude of 0–3.5 km a.s.l., we have used the BC vertical profile within 2.5–10 km a.s.l. observed during the California Air Resources Board (CARB) campaign (Koch et al., 2009) as a representative BC vertical distribution in the free troposphere over California. The CARB vertical profile was scaled so that the averaged BC concentration within 2.5–3.5 km a.s.l. determined from CARB measurements matched CalNex measurements.

The calculated BC optical properties and observed vertical profiles were subsequently used as input to the Fu–Liou–Gu (FLG) RTM (Gu et al., 2006, 2010) to compute the instantaneous clear-sky BC DRF at the top-of-atmosphere. The FLG RTM combines the delta-four-stream approximation for solar flux calculations (Liou et al., 1988) and the delta-two/four-stream approximation for infrared fiux calculations (Fu et al., 1997) to balance accuracy and efficiency. The solar (0–5 µm) and infrared (5–50 µm) spectra are divided into 6 and 12 bands, respectively, based on the location of absorption band. The correlated k-distribution method (Fu and Liou, 1992) is used to

ACPD
15, 19835–19872, 2015

sort gaseous absorption lines within each band. In this study, we employed the monthly mean Goddard Earth Observing System (GEOS-5) meteorological fields for May 2010 to drive the FLG RTM.

3 Results and discussions

3.1 Fresh BC aggregates (stage I)

Figure 3 shows the extinction, absorption, and scattering cross sections (at 532 nm) of fresh BC aggregates at stage I based on laboratory measurements and theoretical calculations using different BC RI and morphology. For comparison with experimental measurements, the averaged value for theoretical results with upper and lower bounds of BC RIs (i.e., 1.95–0.79*i* and 1.75–0.63*i*) is used unless stated otherwise. The calculated extinction cross sections are consistent (differences $\leq 20\,\%$) with measurements for fresh BC aggregates at stage I with different sizes (i.e., D_{BC} = 155, 245, and 320 nm). The discrepancies between theoretical and measured BC absorption cross sections at stage I increase from 3 to 25 % as BC size becomes larger (Fig. 3). On the contrary, the calculated scattering cross sections at stage I are consistently overestimated for different BC sizes compared with measurements, partly because of uncertainty associated with theoretical calculations for small particles. The scattering measurements also contribute to the discrepancy in view of the fact that the integrating nephelometer misses light scattering signals at near-forward directions (Anderson and Ogren, 1998). We note that the calculated SSA (~ 0.16) of BC aggregates at stage I is within the range of 0.15–0.3 determined from atmospheric observations (Bond and Bergstrom, 2006), while the experimentally measured SSA is smaller than 0.10 due to the relatively open and loosely connected BC aggregate structures (Khalizov et al., 2009a).

Sensitivity calculations show that using a BC RI of 1.75–0.63*i* narrows the gap between calculated and measured scattering cross sections of fresh BC aggregates by

ACPD
15, 19835–19872, 2015

up to a factor of two, while using a BC RI of 1.95–0.79i reduces underestimates in the calculated BC absorption which dominates the extinction at stage I (Fig. 3). We found that the extinction, absorption, and scattering cross sections of fresh BC aggregates can vary by up to 60 %, because of applying the BC RI upper or lower bound, in which scattering is most sensitive. Based on the T-matrix calculations using BC RI of 2–1i and 1.75–0.5i, Liu et al. (2008) showed variation of 50–70 % in BC absorption and scattering cross sections depending on aggregate structures, which is comparable to the results derived in this study. Scarnato et al. (2015) also found a strong dependence of BC absorption on BC RI for uncoated aggregates using the DDA method.

Figure 4 shows the extinction, absorption, and scattering cross sections for different aggregate morphology normalized by BC aggregate cross sections determined from standard calculations at stage I. We found that a 20 % increase in D_f (i.e., more compact structure) decreases BC absorption and scattering cross sections by 20–50 %, with greater reductions for larger BC sizes. Using the DDA method, Scarnato et al. (2013) also found a smaller BC absorption for more compact structures. Liu et al. (2008) applied a T-matrix calculation to show that as D_f increases from 1.5 to 3, the absorption of BC aggregates either decreases monotonically or decreases until D_f reaching a certain value and then increases, depending on BC RI, size and the number of primary spherules. This is because the amount of BC directly exposed to the incident light becomes smaller as D_f increases, while the growing interaction among primary spherules could increase light absorption (Liu et al., 2008). The present calculations illustrated that BC absorption and scattering are weakly dependent on the size of primary BC spherules. An increase in the spherule diameter from 15 to 20 nm results in less than 10 % variation in BC extinction, absorption, and scattering cross sections (Fig. 4), which is consistent with the T-matrix results presented by Liu and Mishchenko (2007) who concluded that the monomer size has a rather weak effect on BC scattering and absorption, if fractal dimension is fixed. Nevertheless, the effect of monomer size on BC optical properties could vary significantly depending on BC aggregate shape, size, the number of primary spherules, and BC RI (Liu et al., 2008; Kahnert

ACPD
15, 19835–19872, 2015

et al., 2014). Assuming a volume-equivalent BC sphere instead of fractal aggregates results in 5–25 % weaker absorption and extinction and up to 65 % smaller scattering cross sections for different BC sizes, compared with BC aggregates in standard calculations. The stronger absorption and scattering from aggregate structures is due primarily to the interaction between neighboring primary spherules of BC aggregates (Fuller, 1995). The present calculated increase (5–20 %) in absorption from sphere to aggregate structures is slightly smaller than the value (~ 30 %) reported by Bond and Bergstrom (2006), because of different numbers and sizes of primary spherules, aggregate shapes, and fractal dimensions employed in calculations (Iskander et al., 1991; Liu et al., 2008; Kahnert et al., 2014). Using the T-matrix method, Kahnert and Devasthale (2011) showed a two times higher radiative forcing of BC aggregates than the volume-equivalent sphere counterparts.

3.2 Coated BC particles (stages II and III)

The extinction, absorption, and scattering cross sections (at 532 nm) of coated BC particles at aging stages II and III determined from laboratory measurements and theoretical calculations are depicted in Fig. 3. The theoretical results using upper and lower bounds of BC RI are averaged for comparison with experimental measurements unless stated otherwise. The calculated cross sections of coated BC at stages II and III are in good agreement (differences ≤ 20 %) with laboratory measurements for extinction, absorption, and scattering, except for a 30 % underestimate in scattering for D_{BC} of 320 nm at stage III. This implies that the concentric core-shell model represents the realistic BC coating morphology reasonably well in this case in view of the observed efficient structure compaction during aging (Zhang et al., 2008). The present sensitivity calculations show that the discrepancy in scattering for D_{BC} of 320 nm at stage III cannot be explained by uncertainties associated with BC RI or coating morphology (Fig. 3), which, however, could be attributed to uncertainty associated with the coating mass of H_2SO_4 and H_2O. We assumed only H_2O condensation during BC hygroscopic growth from stage II to III in the calculation of coating mass, which may not be accu-

ACPD
15, 19835–19872, 2015

rate considering that H_2SO_4 condenses on BC surface simultaneously along with H_2O. A sensitivity calculation shows that replacing H_2O with H_2SO_4 in the coating material reduces the discrepancy in scattering to 10 % in this case, since H_2SO_4 is more reflective than H_2O. This also explains the consistent underestimates in the calculated scattering cross sections at stage III for three D_{BC} cases (Fig. 3).

Theoretical calculations show that using BC RI of 1.95–0.79*i* (1.75–0.63*i*) increases (decreases) scattering and absorption cross sections of coated BC particles at stages II and III by up to 30 %, where scattering is most sensitive to BC RI change. We found that the effect of BC RI on extinction and absorption for coated BC particles is similar for different BC sizes, but much smaller than the case of fresh BC aggregates.

Figures 5 and 6 show the extinction, absorption, and scattering cross sections for different coated BC structures normalized by cross sections of the concentric core-shell structure determined from standard calculations. The off-center core-shell structure has little impacts on BC optical properties at stage II (Fig. 5) with differences of less than 10 % compared with the concentric core-shell structure, primarily because of the thin coating layer. As the coating thickness increases after hygroscopic growth, the off-center core-shell structure results in a 5–30 % decrease in extinction, absorption, and scattering cross sections at stage III (Fig. 6). This finding is consistent with the result presented by Adachi et al. (2010) using the DDA method, where they found up to 30 % reductions in BC absorption depending on the position of BC core inside coating material. A recent T-matrix study (Mishchenko et al., 2014) also showed that the absorption of BC-water mixture tends to decrease as a BC particle moves from the droplet center to the boundary.

Compared with the concentric core-shell structure, the closed-cell structure tends to have stronger absorption and weaker scattering for D_{BC} of 245 and 320 nm at stages II and III, while the reverse is true for the open-cell structure (Figs. 5 and 6). This is in line with the conclusion presented in Liou et al. (2011) that closed-cell aggregates have larger absorption and smaller SSA than their open-cell counterparts. The closed-cell structure has a larger surface area for interaction of the incident light with each

ACPD
15, 19835–19872, 2015

primary spherule that acts as a coated core-shell unit, leading to a stronger lensing effect and thus stronger absorption compared with the concentric core-shell structure. However, the open-cell structure lacks a closed coating structure to produce efficient lensing effects. The coating spherules sticking to pure BC spherules in the open-cell structure increase the interaction between the incident light and non-absorbing coating material, resulting in a stronger scattering.

The extinction and absorption cross sections of partially encapsulated and externally attached structures are consistently lower than those of the concentric core-shell structure by 30–80 % for different BC sizes (Figs. 5 and 6). This is because the relatively open coating structure leads to inefficient lensing effect for partially encapsulated and externally attached structures, in which a part of BC aggregates is shielded from interaction with incident photons that are backscattered by the attached non-absorbing coating material. Adachi et al. (2010) showed that the concentric core-shell structure has a 20–30 % stronger absorption than BC aggregates that are fully embedded within host sulfate. Thus, the partially encapsulated structure with only a part of BC aggregates embedded inside coating material in the present study could further decrease the absorption and lead to much smaller absorption values than a concentric core-shell structure. Kahnert et al. (2013) found that the difference in BC absorption between concentric core-shell and encapsulated structures strongly depends on particle size, BC volume fraction, and wavelength, based on the DDA calculation. Interestingly, we found that the absorption of partially encapsulated structure is 10–40 % weaker than that of externally attached structure with larger differences for thicker coating, while their scattering cross sections are similar (differences ≤ 5 %). The preceding analysis demonstrates that coating structures exert a significant impact on BC optical properties. Thus, in order to produce reliable and accurate estimates of BC radiative forcing in climate models, the development of a realistic BC coating morphology parameterization appears to be essential.

ACPD
15, 19835–19872, 2015

3.3 Evolution of BC absorption and scattering

Figure 7 shows the enhancement in absorption and scattering during BC aging from freshly emitted aggregates (stage I) to BC coated by H_2SO_4 (stage II) and by H_2SO_4-H_2O (stage III) for different BC coating structures and sizes. The measured BC absorption increases by 10–45 % due to coating, while the concentric core-shell model results in a 20–65 % absorption increase depending on BC sizes and aging stages. This implies that assuming a concentric core-shell shape could overestimate BC radiative forcing. Adachi et al. (2010) found that using a more realistic BC coating morphology from field measurements leads to about 20 % less BC DRF than using a concentric core-shell shape.

Moreover, coated BC particles with closed-cell structures enhance absorption by 50–100 % for stage II and more than 100 % after hygroscopic growth (Fig. 7). In contrast, the open-cell structures produce less than 10 % increase in absorption during aging for D_{BC} of 245 and 320 nm, while the enhancement tends to be stronger for smaller BC size (D_{BC} = 155 nm). Surprisingly, we found that the partially encapsulated and externally attached BC structures have a weaker absorption than fresh BC aggregates, probably because that the two structures in the absence of fully embedded shape have no efficient lensing effect and that the non-absorbing coating material blocks the photons coming from behind BC aggregates and produces a shadowing effect (Liu and Mishchenko, 2007). This shadowing effect could also explain the decreasing BC absorption for partially encapsulated, externally attached, and open-cell structures when coating material increases during stages II to III. Adachi and Buseck (2013) and Scarnato et al. (2013) found that BC particles attached to or partially immersed in host material, instead of fully embedded within them, do not show noticeable increases in BC absorption relative to uncoated aggregates based on DDA calculations. Bond et al. (2006) recommended a 50 % increase in BC absorption to account for the averaged coating effect during atmospheric aging. However, in light of the preceding analysis, the morphology, composition and amount of coating play significant roles in altering

ACPD
15, 19835–19872, 2015

the BC optical properties during aging. It appears that a fixed enhancement factor may not represent the realistic increase in BC absorption due to complex coating, particularly over regions with highly heterogeneous aging conditions.

Compared with absorption enhancement, BC coating results in a much larger increase in scattering, with a greater enhancement for a larger amount of coating material (Fig. 7). The measured scattering cross sections for different BC sizes increase by a factor of 5–6 from stage I to II and a factor of 11–12 from stage I to III. The calculated increase in scattering from stage I to II varies from a factor of 3 to 8 for D_{BC} of 245 and 320 nm depending on coating morphology, while both the magnitude and variation of enhancement are much larger for D_{BC} of 155 nm ranging from a factor of 6 to 15. After hygroscopic growth (stage III), BC scattering further increases by 20–200 % for different coating structures relative to that at stage II. Cheng et al. (2009) observed that the increase in BC scattering due to coating can reach up to a factor of 8–10 within several hours' aging at a polluted site in northeastern China, which is comparable to laboratory measurements and theoretical calculations presented above.

4 Implication for regional radiative forcing analysis

Figure 8 presents the evolution of BC coating fraction and thickness, optical properties, and DRF during the transport from the source region (LA Basin) to ~ 200 km downwind regions during the CalNex 2010 campaign, including West and East LA Basin, Banning Pass, Banning Outflow, and Imperial Valley. The observed BC loads decrease by a factor of three during transport (Fig. 8c) as a result of the dilution by cleaner air, while the observed BC coating thickness and fraction increase by a factor of two (Figs. 8a, b) revealing a strong BC aging during transport (Metcalf et al., 2012). The present calculations show that the effective BC MAC (i.e., the sum of coated and uncoated BC MAC weighted by their mass fractions) and SSA increases from 10 to 13 $m^2 g^{-1}$ (Fig. 8d) and 0.4 to 0.6 (Fig. 8e), respectively, due to coating during aging. The BC DRF increases from 1.5 to 1.7 $W m^{-2}$ from West to East LA Basin and decreases rapidly to

ACPD
15, 19835–19872, 2015

$\sim 1.0\,W\,m^{-2}$ from East LA Basin to Imperial Valley (Fig. 8f), which is associated with the absorption enhancement produced by coating that dominates the DRF-increasing period and BC concentration dilution that dominates the DRF-decreasing period. The BC DRF over the LA Basin and downwind regions in this case is more than a factor of two higher than the annual mean value over California (Wang et al., 2014) and a factor of 1.5–2 higher than the global annual mean value (Bond et al., 2013). The present analysis shows that the BC DRF varies by 20 % due to the use of upper and lower bounds of BC RI and by a factor of two depending on different BC morphology (Fig. 8f). Thus, it is important to incorporate a realistic representation of BC structure and its parameterization in climate models in order to accurately capture regional BC DRF evolution.

In this conjunction, many global atmospheric models tend to use a fixed BC MAC for DRF estimates in the absence of BC aging microphysics (e.g., Schulz et al., 2006; Wang et al., 2014). We found that using a fixed BC MAC of $11.3\,m^2\,g^{-1}$ that represents the mean BC mixing state from atmospheric observations (Bond et al., 2006), the BC DRF decreases monotonically from 2.1 to $0.8\,W\,m^{-2}$ from the LA Basin to downwind regions, with up to 40 % differences in individual subregions, as compared with the DRF determined from the evolved BC MAC accounting for the change of BC optical properties during aging. Consequently, a fixed BC MAC for the mean mixing state may not be representative and sufficiently accurate within the context of regional radiative forcing analysis, which would require the use of a dynamic BC aging process coupled with the evolution of radiative properties in climate models.

5 Conclusions

We developed a theoretical model that accounts for three typical BC aging stages, including freshly emitted aggregates, coated BC by soluble material, and coated BC particles after further hygroscopic growth. The GOS approach was used to compute BC absorption and scattering at each aging stage, which was coupled with a stochas-

ACPD
15, 19835–19872, 2015

tic procedure to construct different BC structures. The theoretical calculations were compared with laboratory measurements, followed by a systematic analysis on uncertainties associated with BC RI and morphology. Finally, we applied the theoretical aging model and GOS approach to investigate the evolution of BC radiative properties and DRF during the transport from the LA Basin to downwind regions, based on the CalNex 2010 field measurements.

Theoretical calculations yielded consistent extinction (sum of absorption and scattering) cross sections for fresh BC aggregates at stage I, with differences of less than 20 % compared with measurements. Theoretical calculations underestimated BC absorption by up to 25 %, while overestimated BC scattering for different sizes, because of uncertainties involved with both theoretical calculations for small particles and scattering measurements in laboratory experiments. Sensitivity calculations showed that variation of optical cross sections of fresh BC aggregates can be up to 60 % due to the use of different BC RI, in which the scattering is most sensitive. We also found that the optical cross sections of BC aggregates are sensitive to D_f, but insensitive to the size of primary spherules. Using volume-equivalent spheres instead of aggregates decreased the BC absorption at stage I.

The measured extinction, absorption, and scattering cross sections of coated BC were captured (differences $\leq$ 20 %) by theoretical calculations using a concentric core-shell structure for stages II and III, although the scattering at stage III for D_{BC} of 320 nm was underestimated by about 30 % because of uncertainties associated with H_2SO_4-H_2O coating mass. Sensitivity analyses showed that the effects of BC RI on extinction and absorption for coated BC were much smaller than that for fresh BC aggregates. The off-center core-shell structure resulted in up to 30 % less absorption and scattering cross sections than the concentric core-shell structure. The open-cell structure tended to have weaker absorption and stronger scattering than the concentric core-shell structure, while the reverse is true for the closed-cell structure. Compared with the concentric core-shell structure, the partially encapsulated and externally attached

ACPD
15, 19835–19872, 2015

structures had substantially smaller absorption and scattering cross sections due to the lack of efficient lensing effects.

Theoretical calculations showed that using a concentric core-shell structure slightly overestimated the measured enhancement in BC absorption during aging. The closed-cell structure led to a factor of two higher increases in BC absorption than measured values, while the open-cell structure did not show a noticeable increase in absorption for D_{BC} of 245 and 320 nm during aging. The partially encapsulated and externally attached coating structures had a weaker absorption than fresh BC aggregates, likely produced by the shadowing effect from non-absorbing coating material as well as the lack of efficient lensing effect. The increase in BC scattering during aging was much stronger than absorption, ranging from a factor of 3 to 24 depending on BC size, morphology, and aging stage. The present analysis suggested that BC morphology and the amount and composition of coating exert significant impacts on the BC optical properties. Therefore, it is critically important to incorporate realistic BC coating properties in climate models for an accurate estimate of BC radiative forcing.

The CalNex field measurements showed a strong BC aging during its transport from the LA Basin to downwind regions. The resulting BC DRF first increased from 1.5 to 1.7 $W m^{-2}$ and subsequently decreased to 1.0 $W m^{-2}$, as a result of the competition between BC absorption increase due to coating and BC concentration dilution. The present results revealed that BC DRF estimate is highly sensitive to BC morphology during aging. Thus, a reliable estimate of BC radiative forcing in climate models would require the representation of a dynamic BC aging process, including realistic coating structures, especially for regional analysis under highly heterogeneous atmospheric conditions.

The Supplement related to this article is available online at doi:10.5194/acpd-15-19835-2015-supplement.

ACPD
15, 19835–19872, 2015

Acknowledgements. This research was supported by the NSF under Grant AGS-0946315 and AGS-1523296, by the DOE Earth System Modeling program under Grant DESC0006742, and by Subcontract S100097 from the Texas A&M Research Foundation, which is sponsored by NASA under Grant NNX11AK39G. Pacific Northwest National Laboratory is operated for DOE by Battelle Memorial Institute under contract DE-AC05-76RL01830. R. Zhang acknowledges the support by the Robert A. Welch Foundation (A-1417). The authors thank all the contributors to the CalNex and CARB field measurements. Users can access the data in this study through the corresponding author.

References

Adachi, K. and Buseck, P. R.: Changes of ns-soot mixing states and shapes in an urban area during CalNex, J. Geophys. Res.-Atmos., 118, 3723–3730, doi:10.1002/Jgrd.50321, 2013.

Adachi, K., Chung, S. H., and Buseck, P. R.: Shapes of soot aerosol particles and implications for their effects on climate, J. Geophys. Res.-Atmos., 115, D15206, doi:10.1029/2009jd012868, 2010.

Anderson, T. L. and Ogren, J. A.: Determining aerosol radiative properties using the TSI 3563 integrating nephelometer, Aerosol Sci. Tech., 29, 57–69, doi:10.1080/02786829808965551, 1998.

Bond, T. C. and Bergstrom, R. W.: Light absorption by carbonaceous particles: an investigative review, Aerosol Sci. Tech., 40, 27–67, doi:10.1080/02786820500421521, 2006.

Bond, T. C., Habib, G., and Bergstrom, R. W.: Limitations in the enhancement of visible light absorption due to mixing state, J. Geophys. Res.-Atmos., 111, D20211, doi:10.1029/2006jd007315, 2006.

Bond, T. C., Doherty, S. J., Fahey, D. W., Forster, P. M., Berntsen, T., DeAngelo, B. J., Flanner, M. G., Ghan, S., Karcher, B., Koch, D., Kinne, S., Kondo, Y., Quinn, P. K., Sarofim, M. C., Schultz, M. G., Schulz, M., Venkataraman, C., Zhang, H., Zhang, S., Bellouin, N., Guttikunda, S. K., Hopke, P. K., Jacobson, M. Z., Kaiser, J. W., Klimont, Z., Lohmann, U., Schwarz, J. P., Shindell, D., Storelvmo, T., Warren, S. G., and Zender, C. S.: Bounding the role of black carbon in the climate system: a scientific assessment, J. Geophys. Res.-Atmos., 118, 5380–5552, doi:10.1002/Jgrd.50171, 2013.

ACPD
15, 19835–19872, 2015

Cappa, C. D., Onasch, T. B., Massoli, P., Worsnop, D. R., Bates, T. S., Cross, E. S., Davidovits, P., Hakala, J., Hayden, K. L., Jobson, B. T., Kolesar, K. R., Lack, D. A., Lerner, B. M., Li, S. M., Mellon, D., Nuaaman, I., Olfert, J. S., Petaja, T., Quinn, P. K., Song, C., Subramanian, R., Williams, E. J., and Zaveri, R. A.: Radiative absorption enhancements due to the mixing state of atmospheric black carbon, Science, 337, 1078–1081, doi:10.1126/science.1223447, 2012.

Cheng, Y. F., Berghof, M., Garland, R. M., Wiedensohler, A., Wehner, B., Muller, T., Su, H., Zhang, Y. H., Achtert, P., Nowak, A., Pöschl, U., Zhu, T., Hu, M., and Zeng, L. M.: Influence of soot mixing state on aerosol light absorption and single scattering albedo during air mass aging at a polluted regional site in northeastern China, J. Geophys. Res.-Atmos., 114, D00g10, doi:10.1029/2008jd010883, 2009.

China, S., Mazzoleni, C., Gorkowski, K., Aiken, A. C., and Dubey, M. K.: Morphology and mixing state of individual freshly emitted wildfire carbonaceous particles, Nat. Commun., 4, 2122, doi:10.1038/ncomms3122, 2013.

China, S., Scarnato, B., Owen, R. C., Zhang, B., Ampadu, M. T., Kumar, S., Dzepina, K., Dziobak, M. P., Fialho, P., Perlinger, J. A., Hueber, J., Helmig, D., Mazzoleni, L. R., and Mazzoleni, C.: Morphology and mixing state of aged soot particles at a remote marine free troposphere site: implications for optical properties, Geophys. Res. Lett., 42, 1243–1250, doi:10.1002/2014gl062404, 2015.

Decesari, S., Facchini, M. C., Matta, E., Mircea, M., Fuzzi, S., Chughtai, A. R., and Smith, D. M.: Water soluble organic compounds formed by oxidation of soot, Atmos. Environ., 36, 1827–1832, doi:10.1016/S1352-2310(02)00141-3, 2002.

Draine, B. T. and Flatau, P. J.: Discrete–dipole approximation for scattering calculations, J. Opt. Soc. Am. A, 11, 1491–1499, doi:10.1364/Josaa.11.001491, 1994.

Fu, Q. and Liou, K. N.: On the correlated K-distribution method for radiative-transfer in nonhomogeneous atmospheres, J. Atmos. Sci., 49, 2139–2156, doi:10.1175/1520-0469(1992)049<2139:Otcdmf>2.0.Co;2, 1992.

Fu, Q., Liou, K. N., Cribb, M. C., Charlock, T. P., and Grossman, A.: Multiple scattering parameterization in thermal infrared radiative transfer, J. Atmos. Sci., 54, 2799–2812, doi:10.1175/1520-0469(1997)054<2799:Mspiti>2.0.Co;2, 1997.

Fuller, K. A.: Scattering and absorption cross-sections of compounded spheres, 2. calculations for external aggregation, J. Opt. Soc. Am. A, 12, 881–892, doi:10.1364/Josaa.12.000881, 1995.

ACPD
15, 19835–19872, 2015

Gangl, M., Kocifaj, M., Videen, G., and Horvath, H.: Light absorption by coated nano-sized carbonaceous particles, Atmos. Environ., 42, 2571–2581, doi:10.1016/j.atmosenv.2007.05.030, 2008.

Gu, Y., Liou, K. N., Xue, Y., Mechoso, C. R., Li, W., and Luo, Y.: Climatic effects of different aerosol types in China simulated by the UCLA general circulation model, J. Geophys. Res.-Atmos., 111, D15201, doi:10.1029/2005jd006312, 2006.

Gu, Y., Liou, K. N., Chen, W., and Liao, H.: Direct climate effect of black carbon in China and its impact on dust storms, J. Geophys. Res.-Atmos., 115, D00k14, doi:10.1029/2009jd013427, 2010.

He, C., Li, Q. B., Liou, K. N., Takano, Y., Gu, Y., Qi, L., Mao, Y. H., and Leung, L. R.: Black carbon radiative forcing over the Tibetan Plateau, Geophys. Res. Lett., 41, 7806–7813, doi:10.1002/2014gl062191, 2014.

Heintzenberg, J.: Fine particles in the global troposphere: a review, Tellus B, 41, 149–160, doi:10.1111/j.1600-0889.1989.tb00132.x, 1989.

Heintzenberg, J. and Covert, D. S.: Size distribution of elemental carbon, sulfur and total mass in the radius range 10^{-6} to 10^{-4} cm, Sci. Total Environ., 36, 289–297, doi:10.1016/0048-9697(84)90279-1, 1984.

Iskander, M. F., Chen, H. Y., and Penner, J. E.: Resonance optical-absorption by fractal agglomerates of smoke aerosols, Atmos. Environ., 25, 2563–2569, doi:10.1016/0960-1686(91)90173-5, 1991.

Jacobson, M. Z.: Strong radiative heating due to the mixing state of black carbon in atmospheric aerosols, Nature, 409, 695–697, doi:10.1038/35055518, 2001.

Jacobson, M. Z.: Effects of biomass burning on climate, accounting for heat and moisture fluxes, black and brown carbon, and cloud absorption effects, J. Geophys. Res.-Atmos., 119, 8980–9002, doi:10.1002/2014JD021861, 2014.

Johnson, K. S., Zuberi, B., Molina, L. T., Molina, M. J., Iedema, M. J., Cowin, J. P., Gaspar, D. J., Wang, C., and Laskin, A.: Processing of soot in an urban environment: case study from the Mexico City Metropolitan Area, Atmos. Chem. Phys., 5, 3033–3043, doi:10.5194/acp-5-3033-2005, 2005.

Kahnert, M. and Devasthale, A.: Black carbon fractal morphology and short-wave radiative impact: a modelling study, Atmos. Chem. Phys., 11, 11745–11759, doi:10.5194/acp-11-11745-2011, 2011.

ACPD
15, 19835–19872, 2015

Kahnert, M., Nousiainen, T., and Lindqvist, H.: Models for integrated and differential scattering optical properties of encapsulated light absorbing carbon aggregates, Opt. Express, 21, 7974–7993, doi:10.1364/Oe.21.007974, 2013.

Kahnert, M., Nousiainen, T., and Lindqvist, H.: Review: model particles in atmospheric optics, J. Quant. Spectrosc. Ra., 146, 41–58, doi:10.1016/j.jqsrt.2014.02.014, 2014.

Kasper, M., Siegmann, K., and Sattler, K.: Evaluation of an in situ sampling probe for its accuracy in determining particle size distributions from flames, J. Aerosol Sci., 28, 1569–1578, doi:10.1016/S0021-8502(97)00031-1, 1997.

Khalizov, A. F., Xue, H. X., Wang, L., Zheng, J., and Zhang, R. Y.: Enhanced light absorption and scattering by carbon soot aerosol internally mixed with sulfuric acid, J. Phys. Chem. A, 113, 1066–1074, doi:10.1021/Jp807531n, 2009a.

Khalizov, A. F., Zhang, R. Y., Zhang, D., Xue, H. X., Pagels, J., and McMurry, P. H.: Formation of highly hygroscopic soot aerosols upon internal mixing with sulfuric acid vapor, J. Geophys. Res.-Atmos., 114, D05208, doi:10.1029/2008jd010595, 2009b.

Khalizov, A. F., Cruz-Quinones, M., and Zhang, R. Y.: Heterogeneous reaction of NO_2 on fresh and coated soot surfaces, J. Phys. Chem. A, 114, 7516–7524, doi:10.1021/Jp1021938, 2010.

Koch, D., Schulz, M., Kinne, S., McNaughton, C., Spackman, J. R., Balkanski, Y., Bauer, S., Berntsen, T., Bond, T. C., Boucher, O., Chin, M., Clarke, A., De Luca, N., Dentener, F., Diehl, T., Dubovik, O., Easter, R., Fahey, D. W., Feichter, J., Fillmore, D., Freitag, S., Ghan, S., Ginoux, P., Gong, S., Horowitz, L., Iversen, T., Kirkevåg, A., Klimont, Z., Kondo, Y., Krol, M., Liu, X., Miller, R., Montanaro, V., Moteki, N., Myhre, G., Penner, J. E., Perlwitz, J., Pitari, G., Reddy, S., Sahu, L., Sakamoto, H., Schuster, G., Schwarz, J. P., Seland, Ø., Stier, P., Takegawa, N., Takemura, T., Textor, C., van Aardenne, J. A., and Zhao, Y.: Evaluation of black carbon estimations in global aerosol models, Atmos. Chem. Phys., 9, 9001–9026, doi:10.5194/acp-9-9001-2009, 2009.

Kondo, Y., Matsui, H., Moteki, N., Sahu, L., Takegawa, N., Kajino, M., Zhao, Y., Cubison, M. J., Jimenez, J. L., Vay, S., Diskin, G. S., Anderson, B., Wisthaler, A., Mikoviny, T., Fuelberg, H. E., Blake, D. R., Huey, G., Weinheimer, A. J., Knapp, D. J., and Brune, W. H.: Emissions of black carbon, organic, and inorganic aerosols from biomass burning in North America and Asia in 2008, J. Geophys. Res.-Atmos., 116, D08204, doi:10.1029/2010jd015152, 2011.

ACPD
15, 19835–19872, 2015

Lack, D. A., Langridge, J. M., Bahreini, R., Cappa, C. D., Middlebrook, A. M., and Schwarz, J. P.: Brown carbon and internal mixing in biomass burning particles, P. Natl. Acad. Sci. USA, 109, 14802–14807, doi:10.1073/pnas.1206575109, 2012.

Liou, K. N., Fu, Q., and Ackerman, T. P.: A simple formulation of the delta-4-stream approximation for radiative-transfer parameterizations, J. Atmos. Sci., 45, 1940–1947, doi:10.1175/1520-0469(1988)045<1940:Asfotd>2.0.Co;2, 1988.

Liou, K. N., Takano, Y., and Yang, P.: On geometric optics and surface waves for light scattering by spheres, J. Quant. Spectrosc. Ra., 111, 1980–1989, doi:10.1016/j.jqsrt.2010.04.004, 2010.

Liou, K. N., Takano, Y., and Yang, P.: Light absorption and scattering by aggregates: application to black carbon and snow grains, J. Quant. Spectrosc. Ra., 112, 1581–1594, doi:10.1016/j.jqsrt.2011.03.007, 2011.

Liou, K. N., Takano, Y., He, C., Yang, P., Leung, L. R., Gu, Y., and Lee, W. L.: Stochastic parameterization for light absorption by internally mixed BC/dust in snow grains for application to climate models, J. Geophys. Res.-Atmos., 119, 7616–7632, doi:10.1002/2014jd021665, 2014.

Liu, L. and Mishchenko, M. I.: Scattering and radiative properties of complex soot and soot-containing aggregate particles, J. Quant. Spectrosc. Ra., 106, 262–273, doi:10.1016/j.jqsrt.2007.01.020, 2007.

Liu, L., Mishchenko, M. I., and Arnott, W. P.: A study of radiative properties of fractal soot aggregates using the superposition *T* matrix method, J. Quant. Spectrosc. Ra., 109, 2656–2663, doi:10.1016/j.jqsrt.2008.05.001, 2008.

Mackowski, D. W. and Mishchenko, M. I.: Calculation of the *T* matrix and the scattering matrix for ensembles of spheres, J. Opt. Soc. Am. A, 13, 2266–2278, doi:10.1364/Josaa.13.002266, 1996.

Martins, J. V., Artaxo, P., Liousse, C., Reid, J. S., Hobbs, P. V., and Kaufman, Y. J.: Effects of black carbon content, particle size, and mixing on light absorption by aerosols from biomass burning in Brazil, J. Geophys. Res.-Atmos., 103, 32041–32050, doi:10.1029/98jd02593, 1998.

Metcalf, A. R., Craven, J. S., Ensberg, J. J., Brioude, J., Angevine, W., Sorooshian, A., Duong, H. T., Jonsson, H. H., Flagan, R. C., and Seinfeld, J. H.: Black carbon aerosol over the Los Angeles Basin during CalNex, J. Geophys. Res.-Atmos., 117, D00v13, doi:10.1029/2011jd017255, 2012.

ACPD
15, 19835–19872, 2015

Mishchenko, M. I., Liu, L., Cairns, B., and Mackowski, D. W.: Optics of water cloud droplets mixed with black-carbon aerosols, Opt. Lett., 39, 2607–2610, doi:10.1364/OL.39.002607, 2014.
Moffet, R. C. and Prather, K. A.: In-situ measurements of the mixing state and optical properties of soot with implications for radiative forcing estimates, P. Natl. Acad. Sci. USA, 106, 11872–11877, doi:10.1073/pnas.0900040106, 2009.
Moteki, N., Kondo, Y., Miyazaki, Y., Takegawa, N., Komazaki, Y., Kurata, G., Shirai, T., Blake, D. R., Miyakawa, T., and Koike, M.: Evolution of mixing state of black carbon particles: aircraft measurements over the western Pacific in March 2004, Geophys. Res. Lett., 34, L11803, doi:10.1029/2006gl028943, 2007.
Nussenzveig, H. M. and Wiscombe, W. J.: Efficiency factors in mie scattering, Phys. Rev. Lett., 45, 1490–1494, doi:10.1103/PhysRevLett.45.1490, 1980.
Pagels, J., Khalizov, A. F., McMurry, P. H., and Zhang, R. Y.: Processing of soot by controlled sulphuric acid and water condensationmass and mobility relationship, Aerosol Sci. Tech., 43, 629–640, doi:10.1080/02786820902810685, 2009.
Popovicheva, O. B., Persiantseva, N. M., Kireeva, E. D., Khokhlova, T. D., and Shonija, N. K.: Quantification of the hygroscopic effect of soot aging in the atmosphere: laboratory simulations, J. Phys. Chem. A, 115, 298–306, doi:10.1021/Jp109238x, 2011.
Qiu, C., Khalizov, A. F., and Zhang, R. Y.: Soot aging from OH-initiated oxidation of toluene, Environ. Sci. Technol., 46, 9464–9472, doi:10.1021/Es301883y, 2012.
Ramanathan, V. and Carmichael, G.: Global and regional climate changes due to black carbon, Nat. Geosci., 1, 221–227, doi:10.1038/Ngeo156, 2008.
Saathoff, H., Naumann, K. H., Schnaiter, M., Schock, W., Mohler, O., Schurath, U., Weingartner, E., Gysel, M., and Baltensperger, U.: Coating of soot and $(NH_4)_2SO_4$ particles by ozonolysis products of alpha-pinene, J. Aerosol Sci., 34, 1297–1321, doi:10.1016/S0021-8502(03)00364-1, 2003.
Santoro, R. J., Semerjian, H. G., and Dobbins, R. A.: Soot particle measurements in diffusion flames, Combust. Flame., 51, 203–218, doi:10.1016/0010-2180(83)90099-8, 1983.
Scarnato, B. V., Vahidinia, S., Richard, D. T., and Kirchstetter, T. W.: Effects of internal mixing and aggregate morphology on optical properties of black carbon using a discrete dipole approximation model, Atmos. Chem. Phys., 13, 5089–5101, doi:10.5194/acp-13-5089-2013, 2013.

ACPD
15, 19835–19872, 2015

Scarnato, B. V., China, S., Nielsen, K., and Mazzoleni, C.: Perturbations of the optical properties of mineral dust particles by mixing with black carbon: a numerical simulation study, Atmos. Chem. Phys., 15, 6913–6928, doi:10.5194/acp-15-6913-2015, 2015.

Schnaiter, M., Horvath, H., Mohler, O., Naumann, K. H., Saathoff, H., and Schock, O. W.: UV-VIS-NIR spectral optical properties of soot and soot-containing aerosols, J. Aerosol Sci., 34, 1421–1444, doi:10.1016/S0021-8502(03)00361-6, 2003.

Schulz, M., Textor, C., Kinne, S., Balkanski, Y., Bauer, S., Berntsen, T., Berglen, T., Boucher, O., Dentener, F., Guibert, S., Isaksen, I. S. A., Iversen, T., Koch, D., Kirkevåg, A., Liu, X., Montanaro, V., Myhre, G., Penner, J. E., Pitari, G., Reddy, S., Seland, Ø., Stier, P., and Takemura, T.: Radiative forcing by aerosols as derived from the AeroCom present-day and pre-industrial simulations, Atmos. Chem. Phys., 6, 5225–5246, doi:10.5194/acp-6-5225-2006, 2006.

Schwarz, J. P., Spackman, J. R., Fahey, D. W., Gao, R. S., Lohmann, U., Stier, P., Watts, L. A., Thomson, D. S., Lack, D. A., Pfister, L., Mahoney, M. J., Baumgardner, D., Wilson, J. C., and Reeves, J. M.: Coatings and their enhancement of black carbon light absorption in the tropical atmosphere, J. Geophys. Res.-Atmos., 113, D03203, doi:10.1029/2007jd009042, 2008.

Sedlacek, A. J., Lewis, E. R., Kleinman, L., Xu, J. Z., and Zhang, Q.: Determination of and evidence for non-core-shell structure of particles containing black carbon using the single-particle soot photometer (SP2), Geophys. Res. Lett., 39, L06802, doi:10.1029/2012gl050905, 2012.

Shiraiwa, M., Kondo, Y., Iwamoto, T., and Kita, K.: Amplification of light absorption of black carbon by organic coating, Aerosol Sci. Tech., 44, 46–54, doi:10.1080/02786820903357686, 2010.

Stratmann, F., Bilde, M., Dusek, U., Frank, G. P., Hennig, T., Henning, S., Kiendler-Scharr, A., Kiselev, A., Kristensson, A., Lieberwirth, I., Mentel, T. F., Poschl, U., Rose, D., Schneider, J., Snider, J. R., Tillmann, R., Walter, S., and Wex, H.: Examination of laboratory-generated coated soot particles: an overview of the LACIS Experiment in November (LExNo) campaign, J. Geophys. Res.-Atmos., 115, D11203, doi:10.1029/2009jd012628, 2010.

Strawa, A. W., Drdla, K., Ferry, G. V., Verma, S., Pueschel, R. F., Yasuda, M., Salawitch, R. J., Gao, R. S., Howard, S. D., Bui, P. T., Loewenstein, M., Elkins, J. W., Perkins, K. K., and Cohen, R.: Carbonaceous aerosol (Soot) measured in the lower stratosphere during POLARIS and its role in stratospheric photochemistry, J. Geophys. Res.-Atmos., 104, 26753–26766, doi:10.1029/1999jd900453, 1999.

ACPD
15, 19835–19872, 2015

Takano, Y., Liou, K. N., Kahnert, M., and Yang, P.: The single-scattering properties of black carbon aggregates determined from the geometric-optics surface-wave approach and the T-matrix method, J. Quant. Spectrosc. Ra., 125, 51–56, doi:10.1016/j.jqsrt.2013.04.006, 2013.
Toon, O. B. and Ackerman, T. P.: Algorithms for the calculation of scattering by stratified spheres, Appl. Optics, 20, 3657–3660, doi:10.1364/Ao.20.003657, 1981.
Videen, G., Ngo, D., and Chylek, P.: Effective-medium predictions of absorption by graphitic carbon in water droplets, Opt. Lett., 19, 1675–1677, doi:10.1364/Ol.19.001675, 1994.
Wang, Q. Q., Jacob, D. J., Spackman, J. R., Perring, A. E., Schwarz, J. P., Moteki, N., Marais, E. A., Ge, C., Wang, J., and Barrett, S. R. H.: Global budget and radiative forcing of black carbon aerosol: constraints from pole-to-pole (HIPPO) observations across the Pacific, J. Geophys. Res.-Atmos., 119, 195–206, doi:10.1002/2013jd020824, 2014.
Wang, Y., Khalizov, A., Levy, M., and Zhang, R. Y.: New directions: light absorbing aerosols and their atmospheric impacts, Atmos. Environ., 81, 713–715, doi:10.1016/j.atmosenv.2013.09.034, 2013.
Weingartner, E., Burtscher, H., and Baltensperger, U.: Hygroscopic properties of carbon and diesel soot particles, Atmos. Environ., 31, 2311–2327, doi:10.1016/S1352-2310(97)00023-X, 1997.
Xue, H. X., Khalizov, A. F., Wang, L., Zheng, J., and Zhang, R. Y.: Effects of dicarboxylic acid coating on the optical properties of soot, Phys. Chem. Chem. Phys., 11, 7869–7875, doi:10.1039/B904129j, 2009.
Yang, P. and Liou, K. N.: Finite-difference time domain method for light scattering by small ice crystals in three-dimensional space, J. Opt. Soc. Am. A, 13, 2072–2085, doi:10.1364/Josaa.13.002072, 1996.
Yang, P. and Liou, K. N.: Light scattering by hexagonal ice crystals: solutions by a ray-by-ray integration algorithm, J. Opt. Soc. Am. A, 14, 2278–2289, doi:10.1364/Josaa.14.002278, 1997.
Zhang, R. Y., Khalizov, A. F., Pagels, J., Zhang, D., Xue, H. X., and McMurry, P. H.: Variability in morphology, hygroscopicity, and optical properties of soot aerosols during atmospheric processing, P. Natl. Acad. Sci. USA, 105, 10291–10296, doi:10.1073/pnas.0804860105, 2008.
Zhang, R. Y., Khalizov, A., Wang, L., Hu, M., and Xu, W.: Nucleation and growth of nanoparticles in the atmosphere, Chem. Rev., 112, 1957–2011, doi:10.1021/Cr2001756, 2012.
Zuberi, B., Johnson, K. S., Aleks, G. K., Molina, L. T., and Laskin, A.: Hydrophilic properties of aged soot, Geophys. Res. Lett., 32, L01807, doi:10.1029/2004gl021496, 2005.

ACPD
15, 19835–19872, 2015

Table 1. BC physical properties used in theoretical calculations[a].

Aging Stage[b]	Pure BC Mobility diameter (nm)	Pure BC Mass (10^{-16}g)	Coating material Species	Coating material Mass (10^{-16}g)	Standard calculation	Sensitivity calculation
I	155 245 320	5.13 13.0 20.3	–	–	BC aggregates with a fractal dimension of 2.1, BC refractive index of 1.95–0.79*i*, and 164/416/651 primary spherules with diameters of 15 nm for three experimental cases, respectively	(1) BC refractive index of 1.75–0.63*i*; (2) Fractal dimension of 2.5; (3) Primary spherule diameter of 20 nm; (4) Single volume-equivalent BC sphere
II	155 245 320	5.13 13.0 20.3	Sulfuric acid (H_2SO_4)	3.67 11.0 17.9	Concentric core-shell coating structures with BC refractive index of 1.95–0.79*i*	(1) BC refractive index of 1.75–0.63*i*; (2) Off-center core-shell structure; (3) Closed-cell structure; (4) Open-cell structure; (5) Partially encapsulated structure; (6) Externally attached structure
III	155 245 320	5.13 13.0 20.3	Sulfuric acid and water (H_2SO_4-H_2O)	7.59 20.7 33.6	Concentric core-shell coating structures with BC refractive index of 1.95–0.79*i*	(1) BC refractive index of 1.75–0.63*i*; (2) Off-center core-shell structure; (3) Closed-cell structure; (4) Open-cell structure; (5) Partially encapsulated structure; (6) Externally attached structure

[a] Particle properties are derived from measurements in laboratory experiments (Zhang et al., 2008) with initial BC mobility diameters of 155, 245 and 320 nm. See text for details.
[b] See Fig. 1 and text for details.

ACPD
15, 19835–19872, 2015

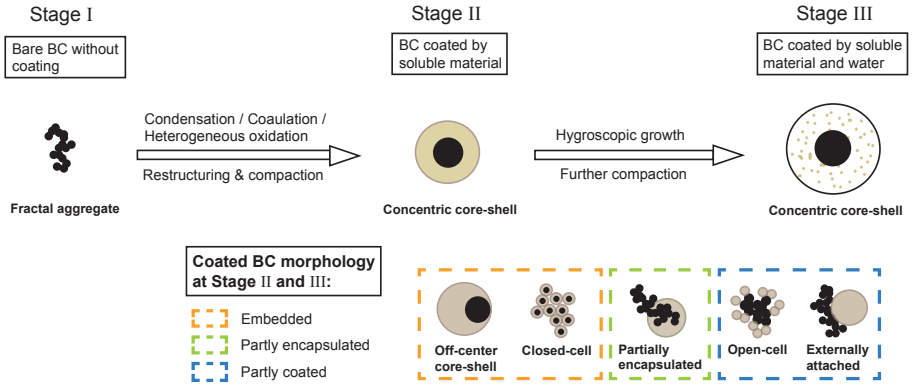

Figure 1. A theoretical model that accounts for three BC aging stages and the associated BC structures, including freshly emitted aggregates (stage I), coated BC by soluble material (stage II), and those after further hygroscopic growth (stage III). Six typical structures for coated BC at stages II and III are considered based on atmospheric observations, including embedded (i.e., concentric core-shell, off-center core-shell, and closed-cell), partially encapsulated, and partly coated (i.e., open-cell and externally attached) structures. See text for details.

ACPD
15, 19835–19872, 2015

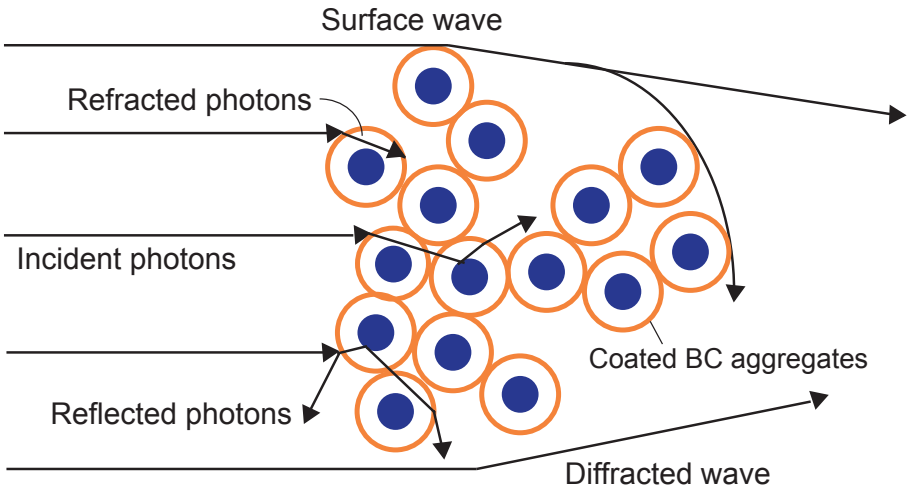

Figure 2. A graphical description of the geometric-optics surface-wave (GOS) approach for light scattering and absorption by coated BC aggregates. The GOS components include the hit-and-miss Monte Carlo photon tracing associated with internal and external refractions and reflections, diffraction following Babinet's principle for randomly oriented irregular particles, and surface waves travelling along the particle edges and propagating into shadow regions. See text for details.

ACPD
15, 19835–19872, 2015

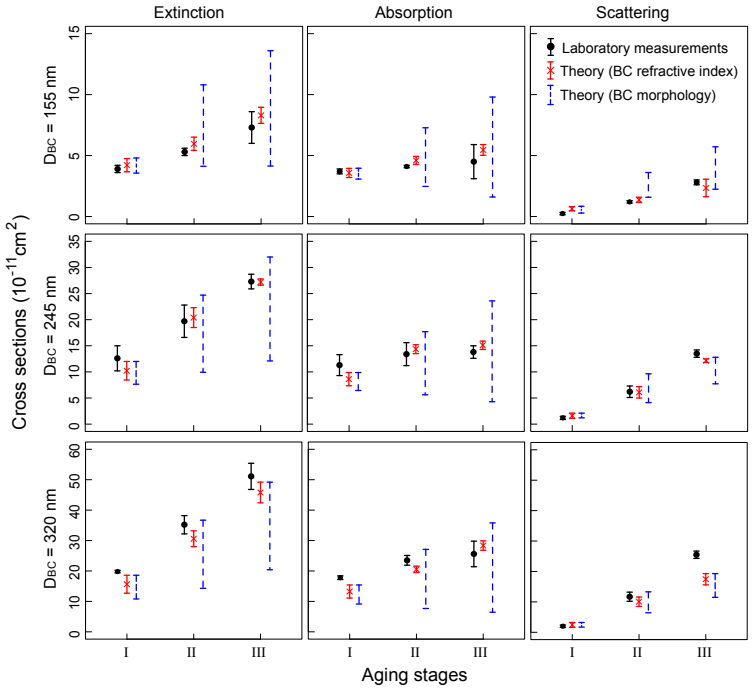

Figure 3. Laboratory measurements and theoretical calculations of BC extinction (left column), absorption (middle column), and scattering (right column) cross sections (at 532 nm) at three aging stages for BC with initial mobility diameters (D_{BC}) of 155 (top row), 245 (middle row), and 320 nm (bottom row). Black circles represent mean values from measurements and black error bars indicate experimental uncertainties reported by Zhang et al. (2008) and Khalizov et al. (2009a). Red crosses represent mean values for theoretical calculations using BC refractive index of 1.95–0.79*i* and 1.75–0.63*i* and red error bars indicate the corresponding upper and lower bounds. Blue error bars represent upper and lower bounds of sensitivity calculations using different BC morphology with refractive index of 1.95–0.79*i* (see also Fig. 1 and Table 1).

ACPD
15, 19835–19872, 2015

Variation of the radiative properties during black carbon aging

C. He et al.

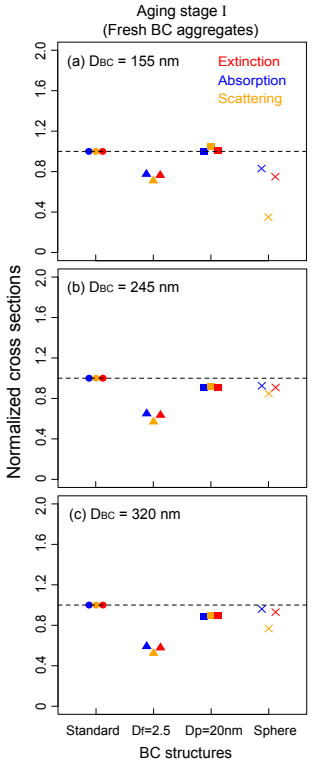

Figure 4. Extinction (red), absorption (blue), and scattering (orange) cross sections (at 532 nm) for different BC morphology normalized by BC aggregate cross sections determined from standard calculations at aging stage I for initial BC mobility diameters (D_{BC}) of 155 nm (top), 245 nm (middle), and 320 nm (bottom). Four BC structures are considered, including BC aggregates in standard calculations (circles), BC aggregates with a fractal dimension (D_f) of 2.5 (triangles; vs. 2.1 in standard calculations), BC aggregates with a primary spherule diameter (D_p) of 20 nm (squares; vs. 15 nm in standard calculations), and a single mass-equivalent BC sphere (crosses; vs. aggregate in standard calculations). Dashed horizontal lines indicate a value of 1.

ACPD
15, 19835–19872, 2015

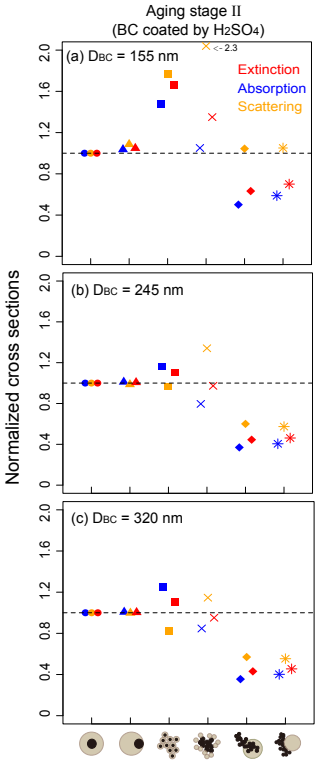

Figure 5. Extinction (red), absorption (blue), and scattering (orange) cross sections (at 532 nm) for different coating morphology normalized by cross sections of concentric core-shell structures determined from standard calculations at aging stage II (BC coated by sulfuric acid (H_2SO_4)) for initial BC mobility diameters (D_{BC}) of 155 nm (top), 245 nm (middle), and 320 nm (bottom). Six BC coating structures are considered, including concentric core-shell (circles), off-center core-shell (triangles), closed-cell (squares), open-cell (crosses), partly encapsulated (diamonds), and externally attached (asterisks) structures (see also Fig. 1). Dashed horizontal lines indicate a value of 1.

ACPD
15, 19835–19872, 2015

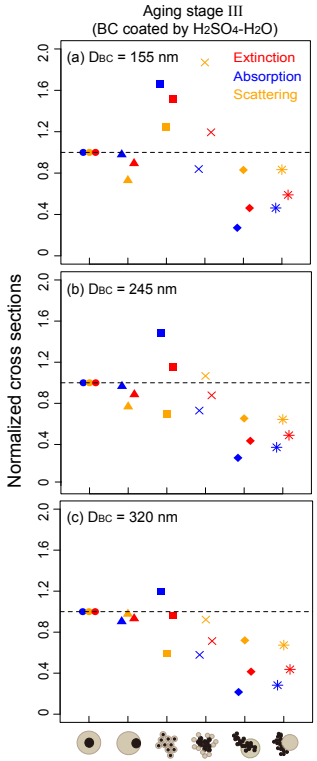

Figure 6. Same as Fig. 5, but for aging stage III where BC particles are coated by both sulfuric acid and water (H_2SO_4-H_2O).

ACPD
15, 19835–19872, 2015

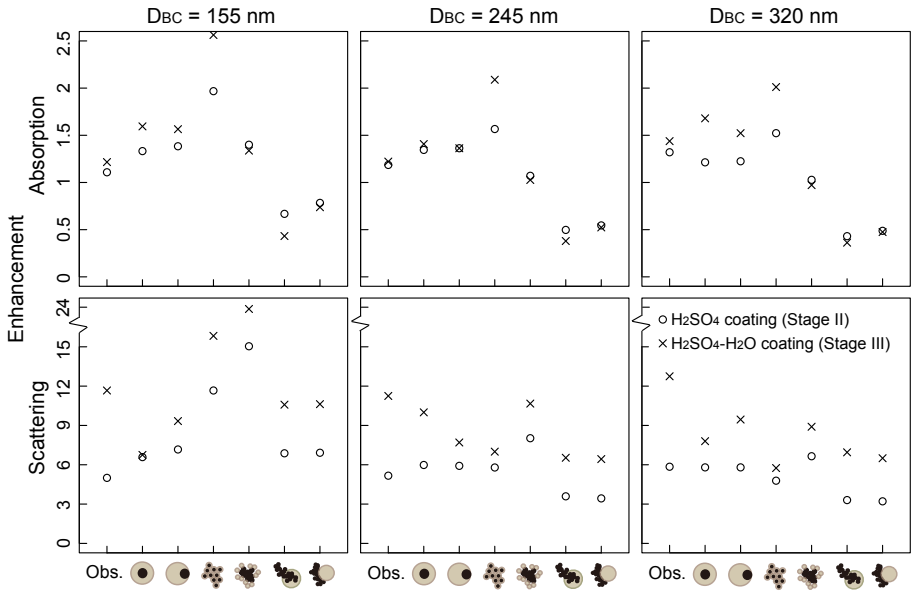

Figure 7. Enhancement in BC absorption (top) and scattering (bottom) during aging from freshly emitted aggregates at stage I to BC coated by sulfuric acid (H_2SO_4) at stage II (circles) and by both sulfuric acid and water (H_2SO_4-H_2O) at stage III (crosses) for initial BC mobility sizes (D_{BC}) of 155 nm (left), 245 nm (middle), and 320 nm (right). The enhancements for different BC coating morphology are shown, including concentric core-shell, off-center core-shell, closed-cell, open-cell, partly encapsulated, and externally attached structures (See also Fig. 1). The enhancement is computed as the ratio of absorption/scattering cross sections of coated BC to the measured values of fresh BC aggregates. Also shown is the measured enhancement from laboratory experiments (Obs.).

ACPD
15, 19835–19872, 2015

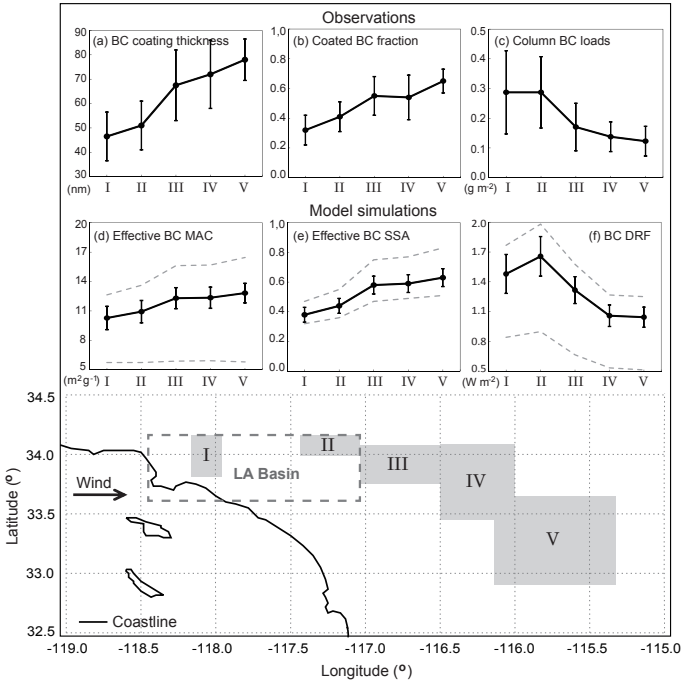

Figure 8. Observations of **(a)** BC coating thickness in diameter, **(b)** fraction of coated BC, and **(c)** column BC loads, and model simulations of **(d)** effective BC mass absorption cross section (MAC), **(e)** effective BC single scattering albedo (SSA), and **(f)** BC direct radiative forcing (DRF) at the top-of-atmosphere over five regions (grey rectangles) during the CalNex 2010 measurements, including (I) West LA Basin, (II) East LA Basin, (III) Banning Pass, (IV) Banning Outflow, and (V) Imperial Valley. Also shown are 1 σ uncertainties (error bars) of observations in **(a)**–**(c)** and the range (error bars) of model results using BC refractive index of 1.95–0.79i and 1.75–0.63i in **(d)**–**(f)**. Dashed grey lines in **(d)**–**(f)** represent upper and lower bounds of model results using different BC morphology (see also Fig. 1 and Table 1) with refractive index of 1.95–0.79i.

ACPD
15, 19835–19872, 2015

Variation of the radiative properties during black carbon aging

C. He et al.